The extreme 2016 wheat yield failure in France

Rogério de S Nóia Júnior, Jean-charles Deswarte, Jean-pierre Cohan, Pierre Martre, Marijn van der Velde, Remi Lecerf, Heidi Webber, Frank Ewert, Alex C Ruane, Gustavo A Slafer, et al.

Received: 15 June 2022 | Revised: 11 December 2022 | Accepted: 8 January 2023

DOI: 10.1111/gcb.16662

Global Change Biology WILEY

RESEARCH ARTICLE

The extreme 2016 wheat yield failure in France

Rogério de S. Nóia Júnior[1] | Jean-Charles Deswarte[2] | Jean-Pierre Cohan[3] | Pierre Martre[4] | Marijn van der Velde[5] | Remi Lecerf[5] | Heidi Webber[6,7] | Frank Ewert[6,8] | Alex C. Ruane[9] | Gustavo A. Slafer[10,11] | Senthold Asseng[1]

[1]Department of Life Science Engineering, Digital Agriculture, HEF World Agricultural Systems Center, Technical University of Munich, Freising, Germany

[2]ARVALIS - Institut du Végétal, Villiers-le-Bâcle, France

[3]ARVALIS - Institut du Végétal, Loireauxence, France

[4]LEPSE, Univ Montpellier, INRAE, Institut Agro Montpellier, Montpellier, France

[5]European Commission, Joint Research Centre, Ispra, Italy

[6]Leibniz-Centre for Agricultural Landscape Research (ZALF), Müncheberg, Germany

[7]Brandenburg Technical University (BTU), Cottbus, Germany

[8]Crop Science Group, INRES, University of Bonn, Bonn, Germany

[9]NASA Goddard Institute for Space Studies, New York, New York, USA

[10]Department of Crop and Forest Sciences, University of Lleida – AGROTECNIO Center, Lleida, Spain

[11]ICREA, Catalonian Institution for Research and Advanced Studies, Barcelona, Spain

Correspondence
Senthold Asseng, Department of Life Science Engineering, Digital Agriculture, HEF World Agricultural Systems Center, Technical University of Munich, Freising, Germany.
Email: senthold.asseng@tum.de

Abstract

France suffered, in 2016, the most extreme wheat yield decline in recent history, with some districts losing 55% yield. To attribute causes, we combined the largest coherent detailed wheat field experimental dataset with statistical and crop model techniques, climate information, and yield physiology. The 2016 yield was composed of up to 40% fewer grains that were up to 30% lighter than expected across eight research stations in France. The flowering stage was affected by prolonged cloud cover and heavy rainfall when 31% of the loss in grain yield was incurred from reduced solar radiation and 19% from floret damage. Grain filling was also affected as 26% of grain yield loss was caused by soil anoxia, 11% by fungal foliar diseases, and 10% by ear blight. Compounding climate effects caused the extreme yield decline. The likelihood of these compound factors recurring under future climate change is estimated to change with a higher frequency of extremely low wheat yields.

KEYWORDS
compounding factors, extreme weather, food security, grain number, grain size, temporally and multivariate events

1 | INTRODUCTION

The production of wheat, the most important source of food for humans (Igrejas & Branlard, 2020), is increasingly variable due to climatic extremes, which threatens to disrupt global efforts toward abolishing poverty and ensuring food security and peace (Nóia Júnior et al., 2021; Perez, 2013; Shew et al., 2020). Europe is responsible for 35% of global wheat production (FAO stat, 2022). Drought and heatwaves are the main causes of the historical crop failures widespread across the breadbasket regions of the continent,

as experienced by northern European countries in 2018 (Beillouin et al., 2020; Webber et al., 2020). Such adverse weather conditions will become more pronounced and widespread with climate change (Battisti & Naylor, 2009; IPCC, 2021; Trnka et al., 2014). For example, in 2010, Russia suffered from the worst heatwave on record according to the Warm Spell Duration Index (Hoag, 2014). Initial attempts have been made to identify the future risk posed by heat and drought to local agriculture (Bailey et al., 2015; Rosenzweig et al., 2013). Several wheat crop modeling approaches have been developed and improved to estimate wheat yield responses to extreme weather conditions (Ceglar et al., 2019; Jägermeyr et al., 2021; Lischeid et al., 2022; Martre et al., 2015; Rötter et al., 2018; Wang et al., 2017; Webber et al., 2017). These studies have helped to identify future regional risks to national and global wheat production directly caused by extreme weather disasters (Asseng et al., 2011; Liu et al., 2019; Webber et al., 2018), and have been incorporated into wheat yield forecast systems to anticipate seasonal food shortages (Bussay et al., 2015; Lecerf et al., 2019; van der Velde & Nisini, 2019).

A major wheat production decline occurred in 2016 in Western Europe, centered around France, the fourth largest wheat-exporting country in the world (Ben-Ari et al., 2018). The national wheat yield of France dropped by 27% in 2016. This was the most extreme wheat yield decline in France since 1960 causing a shortfall of about 2.3 billion $USD in the country's trade balance (Ben-Ari et al., 2018). The public European forecasting system failed to anticipate the magnitude of this wheat yield loss until shortly before harvest (van der Velde et al., 2020), which has been explained by the complexity (sequence, timing, or connectedness) of likely yield-determining events in 2016. Indeed, the 2016 yield failure was not caused by a single event. Winter wheat usually remains dormant during the cold of winter, flowering in the drier, warmer spring weather. However, the combination of a warm, wet winter and an extended period of precipitation in the spring of 2016 led to a number of simultaneous or consecutive yield-reducing factors, including heavy rainfall, crop diseases, low solar radiation, and anoxia, affecting both grain set and grain filling (Ben-Ari et al., 2018). Temporal and multivariate compound events (Bevacqua et al., 2021; Zscheischler et al., 2020) caused the extreme 2016 wheat yield failure. Most crop modeling approaches only consider seasonal water shortage and heat stress, thus neglecting the connected or compound nature of many extreme climate- (Lischeid et al., 2022; Raymond et al., 2020) and weather-related events on crop growth and development. For example, heavy rainfall may damage fragile flowers, immediately reducing the potential to set grain, while waterlogging the soil and depriving roots of oxygen, simultaneously creating humid conditions that encourage the spread of plant diseases with detrimental effects on grain yield and quality. By not accounting for the complex effects or concurrence of multiple factors, the predictive ability of crop forecast systems for Europe is limited, especially for extreme weather (Ruane et al., 2021; van der Velde et al., 2020).

The inability of crop and statistical models to predict the extremely low 2016 wheat yield in France suggests that we are potentially underestimating the projected impacts of climate change on agriculture (van der Velde et al., 2020; Webber et al., 2020). To improve seasonal forecasting systems, we aimed to quantify the impact on yield formation of the possible causes of the poor 2016 yield in France proposed by Ben-Ari et al. (2018). We used a unique detailed dataset from ARVALIS-Institut du vegetal, with observations from 3512 experimental unit treatments at eight locations across the French breadbasket region over 6 years spanning the 2016 extreme (2014–2019). Multi-model regressions, process-based crop growth simulation modeling, and observations of yield physiology were used to separate and quantify various climate impacts on the main wheat yield components in 2016, comparing locations and seasons. We then extended the analysis based on long-term climate change scenarios—from the recent Coupled Model Intercomparison Project phase 6 (CMIP6) climate model ensemble for 2020 to 2100—to analyze the frequency of future concurrent or consecutive weather events potentially causing similar compound yield losses in France.

2 | MATERIALS AND METHODS

The breadbasket of France, accounting for around 70% of France's total wheat production, extends over 27 departments, all impacted by the extreme yield losses in 2016 (Figure 1). ARVALIS-Institut du Végétal wheat field trial data from 3512 experimental unit treatments of 221 cultivars for six cropping seasons (2014–2019 harvests) at eight locations across the breadbasket region were used to quantify the individual contribution of nitrogen leaching, plant diseases, low solar radiation, anoxia, and high rainfall to variation in wheat yield in France in 2016.

2.1 | ARVALIS-Institut du Végétal field trial management

The experimental unit treatments in the 2014–2019 field trials designed and performed by ARVALIS-Institut du Végétal for different objectives were useful in analyzing the following specific aspects (Figure 2).

- Growth performance: 3188 experimental unit treatments tested the performance of a total of 221 winter wheat cultivars in eight research stations, here named 1 to 8 according to the magnitude of wheat yield loss (Figure 1). We used 738 of these experimental unit treatments (which included 172 in 2016) to compute yield component anomalies and develop grain number and grain size statistical models. Only cultivars that had experimental unit treatments in 2016 and in at least one additional year were considered to ensure any yield anomaly was independent of the research station and department (Figure S27). The number of experimental unit treatments per research station is shown in Table S1. In addition, we tested the DSSAT-Nwheat (Kassie et al., 2016) crop simulation model with 42 wheat experimental unit treatments for simulating wheat yield of the winter wheat cultivar Rubisko

(Figures S30 and S31). Growth performance experiments had two types of experiments:

- Cultivar comparison: with around 92% of data, and in all research stations. The objective of these experiments is to compare the growth of several commonly used and developing wheat cultivars. Measurements of wheat ear emergence date, grain number per unit area, average single grain size, grain nitrogen concentration, and grain yield were performed. For these experiments, the flowering date was simulated considering a linear relationship with the ear emergence date, as presented in Figure S28.
- Observatory: with around 8% of data, and in all research stations. The objective of these experiments is to perform a detailed performance measurement of the most common cultivars with greater prospects for use. Measurements of wheat ear emergence and flowering date, total aboveground biomass at anthesis and maturity, total aboveground nitrogen at anthesis, ear density, grain number per unit area, grain number per ear, average single grain size, grain nitrogen concentration, and grain yield were performed.

- Nitrogen response: 124 experimental unit treatments testing the response of wheat cultivars to nitrogen fertilizer rates at research stations 3, 5, and 8. Nitrogen fertilizer rates varied from 0 to 350 kg ha^{-1} (Figure S12). Measurements of wheat ear emergence and flowering date, total aboveground biomass at anthesis and maturity, total aboveground nitrogen at anthesis, ear density, grain number per unit area, grain number per ear, average single grain size, grain nitrogen concentration, and grain yield were performed.
- Plant disease: 2650 experimental unit treatments had records of plant disease types and tests of fungicide efficiency. The efficiency of fungicides was obtained by comparing experimental unit treatments with and without a particular fungicide application. Measurements of wheat yield were performed.

All experimental unit treatments were rainfed and sown from late September to November and harvested between the beginning of July and the end of August. For trials on growth performance and nitrogen response, the crop protection programs were similar to local farm practices which may have included fungicides, herbicides, and insecticides to prevent any damage to the crop. For growth performance and plant disease, nitrogen fertilizer was usually applied in early February, mid-March, and late April, with the total amount applied varying from 175 to 225 kg N ha^{-1}. Phosphorous and potassium fertilizers were applied during autumn if needed to prevent late-season shortage of these nutrients affecting nitrogen uptake, yield, and grain quality.

A single experimental plot was typically 2 m wide and 10 m long, with 11 rows, and the 7 middle rows were harvested. For each experimental unit treatment, we used the average of three single experimental plots, as described by Cohan et al. (Cohan et al., 2019). These field trials sufficiently capture the broader regional impact that occurred in 2016 (Figure S27).

2.2 | Anomalies in wheat yield components

Anomalies in the wheat yield components (WC anomaly) of total aboveground biomass at anthesis and maturity, total aboveground nitrogen at anthesis, ear density, grain number per unit area, average single grain size, grain nitrogen concentration, grain number per ear, and grain yield were calculated based on the 738 growth performance trials. Observed data for grain number per unit area, average single grain size, grain nitrogen concentration, and grain yield were available for all these trials. However, only 40% of the trials had observed data for grain number per ear, and only 10% had observed data for total aboveground biomass at anthesis and maturity, total aboveground nitrogen at anthesis, and ear density.

No WC anomaly was found for total aboveground biomass at anthesis at research stations 2 and 3, or for ear density and grains per ear at research station 2.

For each yield component, the 2016 WC anomaly relative to the 2014–2019 (omitting 2016) reference period was calculated as:

$$\text{WC anomaly}_{(ij)} = \frac{1}{C_{(ij)}} \sum_{k=1}^{C_{(ij)}} \frac{\text{WC}_{2014-2019\ (ijk)} - \text{WC}_{2016\ (ijk)}}{\text{WC}_{2014-2019\ (ijk)}} \quad (1)$$

where $\text{WC}_{2014-2019\ (ijk)}$ and $\text{WC}_{2016\ (ijk)}$ are the wheat yield components for the *i*th research station for the 2014–2019 reference period and the year 2016, respectively, *j*th represents the different wheat yield components, and *C* is the number of cultivars, each individually represented by *k*th.

2.3 | Analysis of the causes of the 2016 anomalies of grain number per unit area and average single grain size

To identify the causes of the 2016 wheat yield failure, we first analyzed the climatic anomalies that occurred across the research stations in France, and noticed that a remarkably wet and warm winter was followed by increased rainfall in late spring, around the time of wheat anthesis. We created indices to analyze the effect of excessive rainfall, low solar radiation, and anoxia, as shown in Tables S2 and S3. We also analyzed the possibility that nitrogen leaching may have affected crop nitrogen uptake, as shown in Section 2.3.1. According to the frequency of diseases observed in the plant disease trials, wheat fusarium ear blight (*Microdochium nivale*), septoria leaf blotch (*Zymoseptoria tritici*), and leaf rust (*Puccinia striiformis* f. sp. *tritici*) were the main diseases of the 2016 wheat-cropping season. Oidium (*Blumeria graminis*) was reported in 0.2% of all the experimental unit treatments and considered not significant for the wheat yield losses of 2016.

The potential contribution of plant diseases, anoxia, heavy rainfall, and nitrogen leaching to the poor 2016 wheat yield was individually analyzed, and separated into those that occurred around anthesis (thus affecting wheat grain number per unit area) and those that occurred during grain filling (thus affecting average single grain size).

2.3.1 | Effects of nitrogen leaching on wheat yield

To determine if nitrogen leaching caused nitrogen deficit stress on plants, we analyzed the results of the nitrogen response and growth performance trials. With these data, the nitrogen nutrition index (NNI), proposed by Justes et al. (1994), was calculated at anthesis for each research station and cropping season, as follows:

$$NNI = \frac{\%N}{\%N_c} \quad (2)$$

where %N ($g\,N\,100\,g^{-1}$ DM) is the nitrogen concentration in the aboveground biomass at anthesis, and $\%N_c$ is the critical nitrogen concentration, calculated as:

$$\%N_c = 5.35 \times Biomass_{ant}^{-0.442} \quad (3)$$

where $Biomass_{ant}$ ($t\,N\,ha^{-1}$) is the total aboveground biomass at anthesis. The crop nitrogen status (Justes et al., 1994) is considered optimal when NNI equals 1, limiting when <1, and "luxury" when >1.

To assess whether crop nitrogen uptake was affected in 2016, the mass of nitrogen that had been taken up by the crops at anthesis and the mass of nitrogen that was translocated from the aboveground vegetative tissues to grains during the grain-filling period were calculated for the years 2016 to 2019 (Figure S13), based on the nitrogen content in straw and grain measured in the experimental unit treatments during these years. Nitrogen leaching was also simulated with DSSAT-Nwheat (see Section 2.4.3) to verify whether the crop simulation model simulated impacts on yield even under nitrogen leaching conditions (Figure S11).

2.3.2 | Effects of solar radiation, rainfall, plant diseases, and anoxia on grain number per unit area and average single grain size

Wheat grain number per unit area is closely related to growing conditions before and shortly after anthesis (Fischer, 1985), when the number of fertile florets is determined and when fertile florets set grains (Slafer et al., 2015). Therefore, solar radiation, rainfall, and temperature conditions were analyzed together with the modeled impact of plant diseases on grain number per unit area for the period around anthesis for each wheat cultivar and each location. The impact of fungal foliar diseases on grain number was not considered because differences between resistant and non-resistant cultivars were not observed in the field experiments (Figure S15). Plant diseases and anoxia were considered as causes of the average single grain size anomaly, as they mostly occurred during the grain-filling period in June and July. Both, septoria leaf blotch and leaf rust are favored by warm, wet winters and wet springs (te Beest et al., 2009), and their impacts were calculated together here as "fungal foliar diseases."

Weather-based indices for low solar radiation, heavy rainfall, and anoxia, as well as other indexes, such as a photo-thermal quotient, were built using daily records of accumulated rainfall (mm), maximum and minimum air temperature (°C), and solar radiation ($MJ\,m^{-2}\,day^{-1}$) from weather stations located close to each research stations. These weather-based indices were created considering wheat phenology, and further details on how these indices were developed and their equations are presented in Tables S2 and S3. Relevant plant disease infection rate models were originally developed and tested by te Beest et al. (2009) for fungal foliar diseases, namely septoria leaf blotch and leaf rust, and for ear blight by Madgwick et al. (2011), we used these models to quantify the incidence of these wheat diseases in France between 2014 and 2019 (Figure S32). Equations and further details of the plant disease models are described in Table S3. These equations were fitted as explanatory variables to calculate grain number per unit area and average single grain size anomalies of 2016.

2.4 | Modeling grain number per unit area and average single grain size anomalies of 2016

2.4.1 | Statistical models

Statistical models were built considering the anomalies of grain number per unit area and average grain size (calculated as in Equation 1) as the objective variables. Weather-based indices for heavy rainfall, solar radiation, and air temperature were used as explanatory variables for grain number per unit area anomalies (Table S2). And weather-based indices for fungal foliar diseases, ear blight, and anoxia, as well as solar radiation and temperature, were the explanatory variables for average grain size anomalies (Table S3). With these weather-based indices, the Gini index (Menze et al., 2009) from the random forest machine learning method was calculated to identify the most influential indices determining grain number per unit area and average single grain size anomalies for 2016 and each of the years of the reference period 2014–2019 (excluding 2016).

A stepwise procedure was then used to select the best combination of input variables for quantifying extreme crop yields (Ben-Ari et al., 2018; Nóia Júnior et al., 2021). These stepwise procedures were also performed in R with the command step. Based on the Gini index, an indicator of the relative importance of the weather-related factors in determining the 2016 anomalies, statistical models were built using the explanatory variables of ear blight, low solar radiation, and high rainfall indices for grain number anomaly of 2016, and fungal foliar diseases, ear blight, low solar radiation, and anoxia during grain filling for grain size anomaly of 2016. The statistical models for grain number or grain size ($\hat{y}_g$) were built as shown in Equation 4:

$$\hat{y}_g = \beta_0 + \beta_1 x_1 + \ \ldots \ + \beta_D x_D \quad (4)$$

where $\hat{y}_g$ is the objective variable (or grain number per unit area anomaly or average grain size anomaly of 2016), β_0 is the estimate of intercept, and $\beta_1$and β_D are the estimates of coefficient for each of the explanatory variables from x_1 and x_D.

The research stations had different numbers of experimental unit treatments (Table S1), and to capture the spatial distribution of grain number and average single grain size anomalies, the statistical models were built 1000 times with parameter values perturbed through random selections of the variables, keeping two experimental unit treatments per research station (the experimental unit treatment values within the same research station usually correspond to different cultivars). Thus, the statistical models were always trained for two experimental units simultaneously in eight research stations, summing up to 16 values of grain number or grain size anomalies fitting their 16 corresponding values of each explanatory variable. The performance of the models (r^2) was computed in a randomly selected grain number or grain size anomaly of 2016 not included in the trained dataset (out-of-sample analysis). The influential weather-based indices were selected using the Akaike information criterion (AIC) independently for each of the 1000 models for grain number per unit area and average grain size. Thus, the final contribution of each index considered in the grain number per unit area and average single grain size anomaly models was assessed with the mean of an ensemble of 1000 statistical models (quantification of the impacts of different indices is detailed and explained in Section 2.4.2).

Grain number and average single grain size were observed in field experiments from 738 (with 172 in 2016) performance trials. Anomalies were calculated from these observed grain numbers and grain sizes.

2.4.2 | Quantifying the impacts of individual yield-limiting factors in 2016

The 1000 models of grain number and grain size anomalies in the 2016 cropping season were executed by initially taking the 2016 values for each input variable (derived from weather-based indices and plant disease model outputs). The models were executed again, but this time, value of an explanatory variable for 2016 was replaced by that for each of the years in the reference period from 2014 to 2019 except 2016 (Figure S29). This step was repeated, replacing the value of each input variable in turn. Thus, the contribution of each factor to the 2016 wheat yield anomaly was calculated as the difference between the estimated grain number or average single grain size values from running the models with all variables for 2016, and the estimates from running the statistical models with all variables of 2016 except one from a reference year (Figure S29). For example, to calculate the contribution of low solar radiation to the grain number per unit area in 2016, all the 1000 models of grain number were executed with all variables (weather-based indices inputs) from the 2016 cropping season. At the same time, the same 1000 models were executed with all variables for 2016 but low solar radiation index was from 2014 to 2019 (excluding 2016 and individually executed for each year of the reference period). As a result, there were 6000 grain number anomaly estimates (1000 for 2016 with all variables from 2016 and 5000 for 2016 with modified solar radiation from 2014 to 2019 reference period). The difference between the average of the 1000 estimates for 2016 with all variables from 2016 ("R1: in Figure S29) and the average of the 5000 estimates for 2016 with modified solar radiation from 2014 to 2019 reference period ("R2"–"Rx" in Figure S29) was considered to be the size of the impact of low solar radiation. This procedure was repeated for each input variable (weather-based indices and plant disease model outputs) for grain number per unit area and average grain size. The impacts on yield were computed considering that grain yield is the result of the product of grain number per unit area and average grain size. The calculated impact of each variable was summed up and proportionally divided according to the size of the anomaly of grain number per unit area, average grain size, and grain yield of each location. The residual is considered as the difference between the estimated and observed anomalies (Figures 3h and 4j). Additional details are presented in Text S1.

This is similar to the method proposed by Asseng et al. (2011) for separating the impacts of temperature from other factors on wheat yield. The contribution of each factor calculated with the statistical models was compared with solar radiation impacts simulated by the DSSAT-Nwheat crop simulation model (described in Section 2.4.3, Figure S17) and impact of plant diseases calculated with resistant and sensitive cultivars in the plant disease trials.

Weather-based indices highly correlated as heavy rainfall and anoxia were explanatory variables for different objective variables (heavy rainfall for grain number and anoxia for grain size, as described in Section 2.3.2). The impacts of low solar radiation index (which is correlated with heavy rainfall, both explanatory variables of grain number per unit area) were also quantified with a crop simulation model as an independent analysis.

2.4.3 | DSSAT-Nwheat crop simulation model

The DSSAT-Nwheat process-based crop simulation model used in this study is part of the DSSAT crop modeling framework (https://dssat.net/). DSSAT-Nwheat has been widely tested in wheat modeling growth studies across the world (Kassie et al., 2016). The calibration of DSSAT-Nwheat to the breadbasket region of France was done for cultivar Rubisko grown in the 42 experimental unit treatments in 2014, 2015, 2017, and 2019 (Text S1). Although data from 2016 and 2018 were available, they were not used for calibration because of the high incidence of wheat diseases in these years, which is not simulated by the Nwheat model. The root-mean-square error (RMSE) for total aboveground biomass and grain yield was 0.8 kg ha^{-1} (4%) and 0.6 kg ha^{-1} (6%), respectively. The precision of Nwheat was satisfactory for total aboveground biomass (r^2 = .83) and grain yield (r^2 = .70) (Figure S30). After calibrating, Nwheat was tested for 2016 and 2018 with the result that total aboveground biomass and grain yield were both overestimated (Figure S31). This was expected because Nwheat does not account for how the stress factors of heavy rainfall around anthesis, anoxia, and diseases affect plant growth. However, Nwheat was still used to quantify the solar radiation (Figures S16 and S17) and nitrogen leaching (Figure S11) impacts on wheat grain yield. The calibrated coefficients are shown in Table S4. The impact of low solar radiation with DSSAT-Nwheat was calculated by modifying the 2016

seasonal daily solar radiation inputs with the other years in the reference period 2014–2019, the same as the method applied to statistical models (described in Section 2.4.2).

2.5 | Climate change scenarios

Daily climate data for the 1960–2100 period were drawn from the Inter-Sectoral Impacts Model Intercomparison Project (ISIMIP) (Lange, 2019), which provides bias-adjusted and spatially disaggregated climate model outputs from the Coupled Model Intercomparison Project phase 6 (CMIP6) (Eyring et al., 2016). Historical simulations before 2015 are from climate models forced by the historical trends in the main natural and anthropogenic factors. After 2015, simulations follow the Shared Socioeconomic Pathway and Representative Concentration Pathway SSP5-8.5 (O'Neill et al., 2020). The IPCC describes this as a "very high" emissions scenario (IPCC, 2021), and we use it here to illustrate the upper tail of future risk (analysis was also performed for SSP5-2.6 and the results are shown in Figure S21). We considered five CMIP6 models (GFDL-ESM4, IPSL-CM6A-LR, MPI-ESM1-2-HR, MRI-ESM2-0, and UKESM1-0-LL) that include high, medium, and low climate sensitivity models similar to the full CMIP6 distribution (Jägermeyr et al., 2021). We used daily weather data from the ISIMIP downscaled projections for the five selected models to quantify future frequency of ear blight, foliar fungal diseases, heavy rainfall, low solar radiation around anthesis (with anthesis date fixed at 1 June), and anoxia during wheat grain filling (from 1 June to 31 July) using the indices previously described (Tables S2 and S3) for predicting wheat grain number per unit area and average single grain size anomalies of 2016. To minimize uncertainties related to fixed anthesis and grain-filling periods, we carried out an additional analysis considering different fixed dates of anthesis (with anthesis date fixed at 1 May), and anoxia during wheat grain filling (from 1 May to 15 June) (Figures S19–S34).

The extreme 2016 wheat yield failure occurred once in 62 years from 1960 to 2021, with 1.6% frequency. Similarly, extreme low national wheat yield was here estimated for each GCM separately and defined as the 1st percentile of each wheat yield component during 1960–2020 (which as a 1% frequency is equivalent to once every 100 years), with the grain number and grain size anomaly models used for quantifying the impacts of individual yield-limiting factors in 2016. We averaged the simulated grain number and grain size for the eight research stations to scale-up to the regional level, as suggested by Ben-Ari et al. (2018). Individual results for each research station are presented in Figure S19.

With weather-based index used for building the grain number per unit area and average grain size statistical models (Tables S2 and S3), we refitted a new statistical model to estimate grain yield from 1984 to 2020 in the breadbasket of France (Figure S33). This new statistical model for wheat yield was built as described in Section 2.4.1. We applied the new wheat yield model used to project the future frequency of extremely low wheat yield years in the breadbasket of France and the results are shown in Figure S33b. This was performed to reduce uncertainties of projections for future frequency of the extreme 2016 wheat yield failure in the breadbasket of France.

2.6 | Statistical analysis

All data analyses and statistical analyses were carried out using the statistical program software R (R Core Team, 2017). To analyze the yield component anomalies across research stations, the data were submitted to an analysis of variance (ANOVA) and, when significant, the mean values were compared using the Tukey test. The random forest models were fitted to the data by using the function randomForest of the R package "randomForest." ANOVA (mean of squares) were carried out to determine the degree to which the climatic variables selected by the statistical models could explain wheat grain number per unit area and average single grain size anomalies of 2016 across all the studied research stations (i.e., ANOVA was only computed for 2016 anomaly). Statistically significant differences were judged at alpha = .05. An ANOVA was performed with the function aov. As the statistical models, ANOVA was computed 1000 times. The importance of each variable to explain spatial variation of wheat grain number per unit area and average grain size anomalies in 2016 was calculated as the average of 1000 ANOVA analyses.

3 | RESULTS

3.1 | Extreme yield loss and weather conditions in 2016 in France

The 2015/2016 wheat-growing season in France started with unusually high temperatures, with monthly averages of 3°C above November and December (autumn and early winter) averages for the 2010–2020 period (Figure 1b). Late winter was particularly wet, with accumulated rainfall of 90 mm in March, twice the 2010–2020 average for this month (Figure 1c). After the warm and wet winter, spring 2016 was on average 1.5°C cooler than the average spring temperature of the 2010–2020 period. There was high rainfall from late May to early June in 2016. The accumulated rainfall in this period was the highest recorded in 30 years (Figure S3). Cloud cover associated with the high rainfall led to a 30% decrease in monthly solar radiation in May and June compared to the 2010–2020 average. Low solar radiation and high rainfall continued until early July. The weather conditions in France and other parts of Western Europe in 2016 were similar (Figure 1a; Figures S1 and S2), but the accumulated rainfall in May and June was not uniformly high, as some northwestern areas of France received less rainfall including around research station 8 (Figure S1).

3.2 | Yield components during the wheat-growing season for the 2016 harvest in France

For each of the eight research stations across France, the 2016, anomaly in various wheat growth and yield components was calculated with respect to the 2014–2019 reference period (omitting 2016; Figure 2) from field experiment data. Total aboveground biomass at anthesis (Figure 2a) and ear density (Figure 2b) for 2016 was

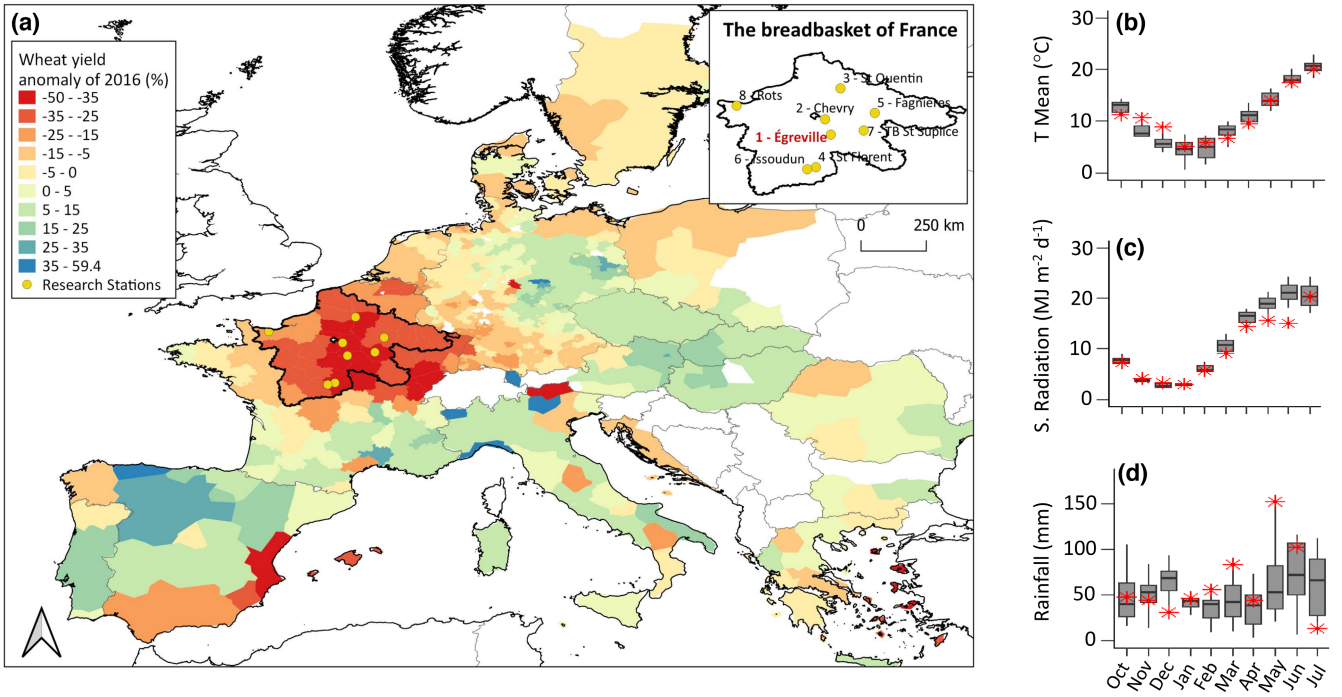

FIGURE 1 Extremely low wheat yields in Western Europe in 2016. (a) Spatial distribution of the observed 2016 trend-corrected wheat yield anomaly. The breadbasket region of France is outlined by bold black contours with locations and names of the research stations (yellow dots) shown also in the inset (upper right). Boxplot of monthly (b) mean temperature (T mean), (c) solar radiation, and (d) rainfall, over the wheat-growing season for 2013–2020 harvest years for the most severely affected region at Égreville, France (research station 1). Lower whiskers extend below the 25% quantile (Q1) and upper whiskers above the 75% quantile (Q3) by 1.5 times the interquartile range (interval between Q3 and Q1). Values for the 2015/2016 growing season are plotted as red asterisks. Weather data for the other field sites studied and across Europe are shown in Figures S1–S8. Map lines delineate study areas and do not necessarily depict accepted national boundaries.

similar to those of the reference period averages, with anomalies varying from −10% to 10% at the different research stations. DSSAT-Nwheat crop growth model simulation results suggest that nitrogen leaching in 2016 occurred between the stem elongation and anthesis (Figure S11). Despite this, total aboveground nitrogen at anthesis was up to 25% higher (Figure 2c), and the corresponding nitrogen nutrition index at anthesis was 5%–20% higher in 2016 than during the reference period (Figure 2f).

Observed total aboveground biomass at maturity dropped by as much as 40% (Figure 2d), while grain number per ear and per m^2 fell by as much as 40% and 50%, respectively, in 2016 (Figure 2e,g). A negative anomaly of about 40% in grain size (i.e., average single grain size) was also found for 2016 (Figure 2h) compared with the reference period. As a result, the grain yield loss in 2016 compared to 2014–2019 varied from 15% to 72% according to the research station (Figure 2i), and the greatest loss across a district was 55%.

Wheat yield is the result of wheat grain number and grain size, and their values are indicative of stresses that occur within a season and the timing of those stresses. For example, grain number per unit area is related to growing conditions before and shortly after anthesis (Fischer, 1985), when most fertile florets set grains (Slafer et al., 2015). Therefore, we first identified the growing conditions potentially causing the wheat yield anomaly in 2016, and placed these effects in the phenological context of when they would have occurred.

3.3 | Grain number and extremes of high rainfall and low solar radiation around anthesis

In 2016, anthesis occurred a few days later than usual because the low temperatures of late winter and early spring delayed wheat phenology (Figure 3a,c). The delayed anthesis coincided with abnormally heavy rainfalls (i.e., daily rainfall >20 mm) and low solar radiation in late May and early June (Figure 3b,d). In addition to numerous heavy rainfall events, the accumulated rainfall during the 15 days around anthesis, varying from 45 mm to 180 mm depending on the research station, was up to five times more than expected for the period. Indeed, records show that this was the longest period of rainfall in 30 years. Anthesis occurred during 54 h of almost uninterrupted rainfall (Figure S8) in a week when hourly solar radiation mostly remained below the wheat light compensation point of 50 W m^{-2} (Pang et al., 2018). The 2016 anomaly in grain number per unit area was the most drastic in the research stations receiving more rainfall and less solar radiation around anthesis, and was particularly low for specific cultivars which underwent anthesis just at the time of peak rainfall in this period of maximum daily accumulated rainfall (Figure 3e). For example, the grain number anomaly was −13% for the cultivar Rubisko in research station 8, which is less extreme than the −45% anomaly for this cultivar in research station 1, but more extreme than the decline seen for cultivar Soissons grown in the same research station but which underwent anthesis earlier (Figure 3e).

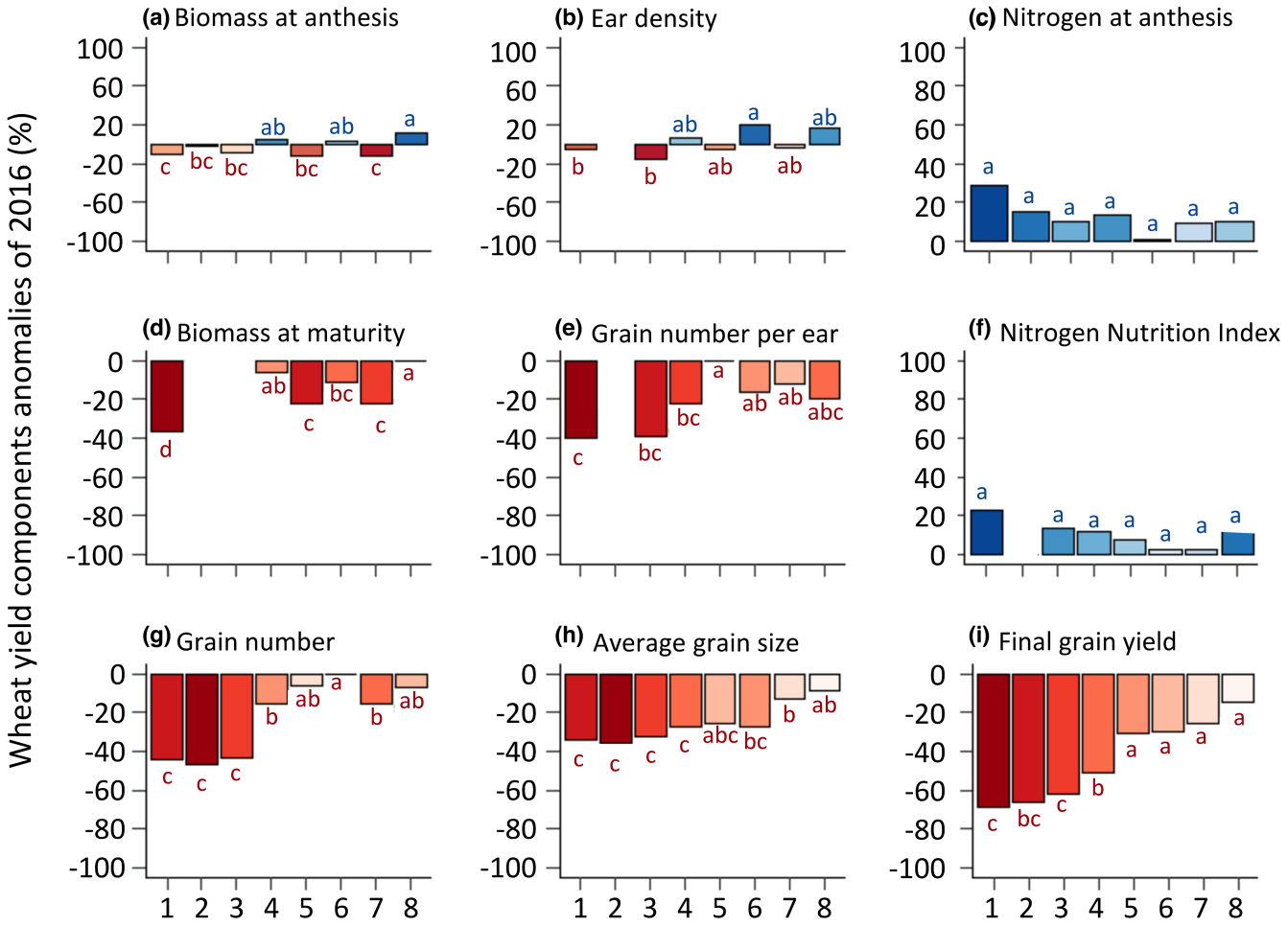

FIGURE 2 Components of 2016 wheat yield anomalies that occurred at eight sites in the main breadbasket of France. Observed positive (blue) and negative (red) anomalies in 2016 in relation to the average for 2014–2019 (omitting 2016) wheat harvests for the growth components, (a) total aboveground biomass at anthesis, (b) ear density (ear number per unit area), (c) total aboveground nitrogen at anthesis, (d) total aboveground biomass at maturity, (e) grain number per ear, (f) nitrogen nutrition index, (g) grain number per unit area, (h) average single grain size, and (i) final grain yield. Different letters within each panel represent statistically significant differences in the component anomaly between the research stations ($p < .05$). For each yield component, bar shading indicates the ranking in magnitude of anomalies (as in i) for each site from the largest (dark) to the smallest (pale). The research stations were numbered from 1 to 8 according to the magnitude of their wheat yield loss in 2016 (as in i, location 1 had the highest yield loss in 2016 and location 8 the lowest): 1, Égreville; 2, Chevry; 3, Saint-Quentin; 4, Saint-Florent; 5, Fagnières; 6, Issoudun; 7, Barbarey-Saint-Sulpice; and 8, Rots.

To assess the impacts of low solar radiation and high rainfall and other possible limiting factors on the 2016 grain number anomaly, we determined the Gini index to show the importance of the variables in a random forest and a multi-model regression model fitted using a stepwise selection procedure. Both the Gini index and the multi-model regressions were calculated 1000 times through random selections of wheat grain number anomalies. Thus, the circular graphs in Figure 3f,g represent the frequency of selection of each limiting factor as the first, second, or third most important variable for explaining wheat grain number in 2016 (Figure 3f) and for the reference period of 2014–2019 (without 2016) (Figure 3g). The photo-thermal quotient (Fischer, 1985) (Table S2) was by far the most important factor for defining wheat grain number per unit area in the 2014–2019 reference period, whereas the variation of grain number among the stations and cultivars in 2016 was explained mainly by the level of solar radiation and heavy rainfall events, both around anthesis. In the multi-model regression models, these variables together explain most of the 2016 anomaly of grain number per unit across the eight locations representative of the breadbasket region of France (Figure 3h).

3.4 | Grain size and plant diseases and anoxia

The autumn and early winter of 2015 were unusually warm, including several days when the mean temperature was 10°C higher than the 2010–2020 average (Figure 4a,c). This was followed by higher-than-normal amounts of precipitation during late winter and early spring, with a total accumulated rainfall of up to 300 mm (Figure 4b,d). Such warm and moist conditions were propitious to foliar diseases and Septoria leaf blotch was observed in 91% and wheat leaf rust in

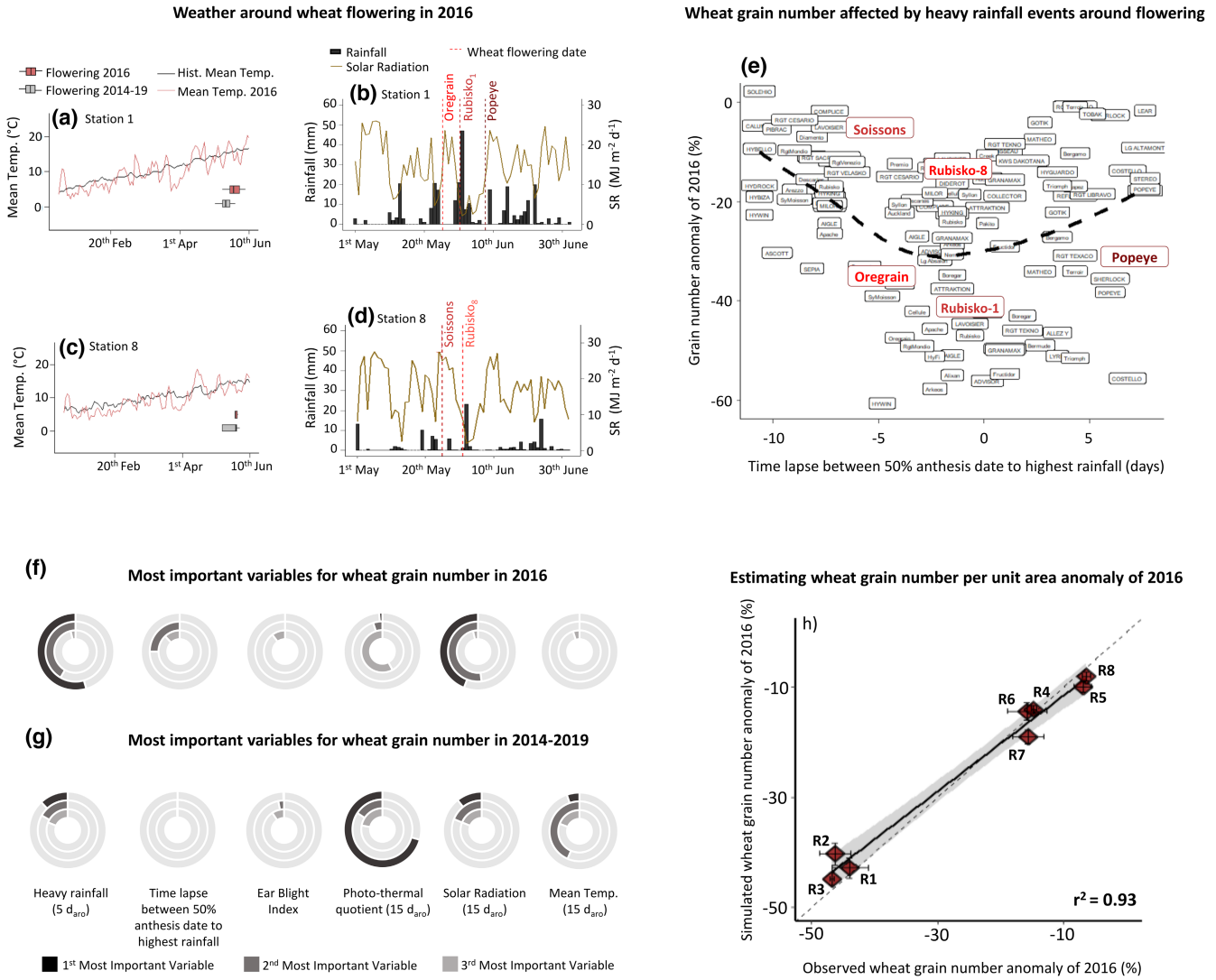

FIGURE 3 Wheat grain number as affected by adverse weather conditions around anthesis. (a–d) Comparison of wheat anthesis date and weather conditions during late winter and spring for 2016 and the mean of 2014–2019 (without 2016) harvests at (a, b) research station 1 and (c, d) research station 8. (a, c) Mean temperature traces with boxplots of anthesis dates of all cultivars grown at each site. (b, d) Daily solar radiation (trace) and accumulated rainfall (bars) with dotted lines indicating the anthesis dates of individual cultivars. (e) Relationship between observed anomaly in grain number of different winter wheat cultivars for the 2016 and 2014–2019 harvests and the time lapse between the date when 50% of individuals had flowered (50% anthesis date) and the day with highest rainfall (see Table S2). (f, g) The three most important variables selected according to the Gini index from 1000 different models estimated from random forest variable selector method for estimating wheat grain number anomalies in France considering (f) only the 2016 harvest, and (g) all harvests from 2014 to 2019 excluding 2016. (h) Comparison between the observed and simulated 2016 wheat grain number per unit area anomaly using a multiple regression linear model, from 1000 different models in an out-of-sample analysis – errors bars show the standard errors from the 1000 simulations (vertical errors bars) and the observed grain number anomaly (horizontal errors bars) in (h). The research stations (R) are as follows: 1, Égreville; 2, Chevry; 3, Saint-Quentin; 4, Saint-Florent; 5, Fagnières; 6, Issoudun; 7, Barbarey-Saint-Sulpice; and 8, Rots.

17% of all experimental unit treatments studied by ARVALIS across the breadbasket region of France (Figure 4g). High rainfall around anthesis led to widespread soil saturation and flooding during the wheat grain-filling period (Figure 4e) and a high incidence of ear blight. Usually marginal, ear blight was observed in 27% of all the experimental unit treatments in 2016 (Figure 4g). Water balance simulations, accounting for the difference between daily reference evapotranspiration and rainfall, indicated an excess of water of up to 120 mm from early June until late July, spanning most of the wheat grain-filling period (Figure 4e). Water was in excess at all the research stations except research station 8, which notably had the smallest yield loss (Figure 4f). The combination of these extreme conditions, plus the stress from disease and anoxia, and limited solar radiation during grain filling, may have affected grain size (Text S1 and Figure S23). The effect of these variables was confirmed by ranking their importance using the Gini index (Figure 4h,i). Overall,

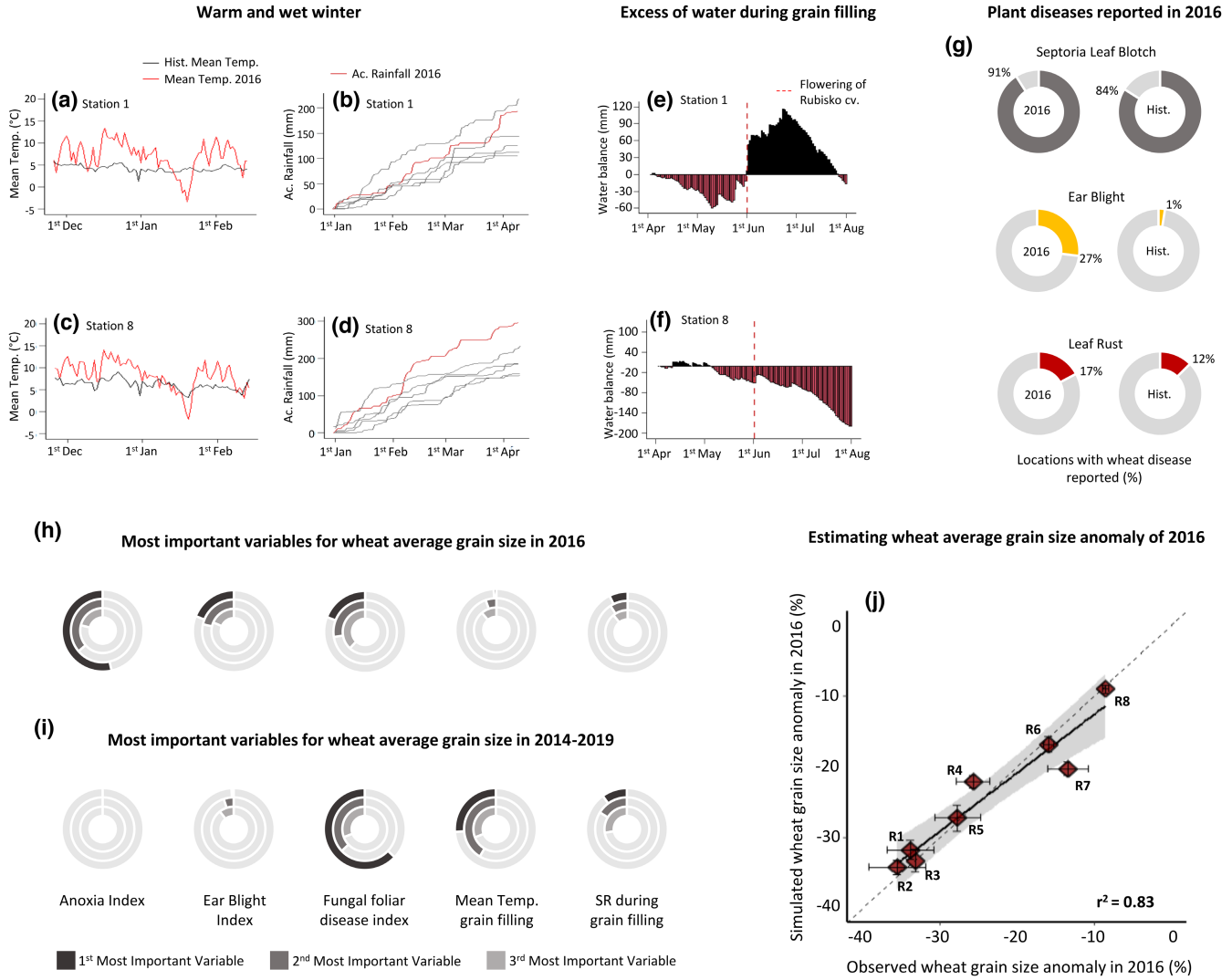

FIGURE 4 Wheat grain size affected by plant diseases and excess water. (a–d) Weather conditions during the 2016 winter at (a, b) research station 1 and (c, d) research station 8. (a, c) Mean temperature in 2016 (red trace) compared to the average (grey trace) for the reference period of 2014–2019 (omitting 2016) and (b, d) daily accumulated rainfall (red trace) compared to other individual years in the reference period of 2014–2019 (grey traces). (e, f) Accumulated daily difference between reference evapotranspiration (ETo) and rainfall (water balance) around anthesis in 2016 in (e) research station 1 and (d) research station 8. Red bars indicate a negative balance, and black bars indicate a positive balance. The flowering time of the Rubisko cultivar at each site is indicated. (f) Frequency of plant diseases reported in ARVALIS plant disease trials across the breadbasket region of France in 2016 compared to the average (Hist.) of 2014–2019 (omitting 2016). (h, i) The three most important variables selected according to the Gini index from 1000 different models estimated from random forest variable selector for estimating average single grain size anomalies considering (h) only 2016, and (i) all the harvests from 2014 to 2019, excluding 2016. (j) Comparison between the simulated and observed 2016 anomaly in average single grain size with a multiple regression linear model, from 1000 different models in an out-of-sample analysis – errors bars show the standard errors from the 1000 simulations (vertical errors bars) and the observed grain size anomaly (horizontal errors bars) in (j). The research stations are as follows: 1, Égreville; 2, Chevry; 3, Saint-Quentin; 4, Saint-Florent; 5, Fagnières; 5, Issoudun; 7, Barbarey-Saint-Sulpice; and 8, Rots.

in multi-model regressions, fungal foliar diseases, ear blight, anoxia, and low solar radiation could explain most of the 2016 anomaly in grain size (Figure 4j).

3.5 | Causes of wheat yield decline in 2016

Based on the skill of the multi-regression models at estimating grain number and grain size anomalies, we extended the analysis to quantify the contribution of each of these factors to the 2016 losses in grain number per unit area, grain size, and grain yield at each research stations (Figure 5). ANOVA results indicated that the 2016 grain number per unit area anomaly was mainly caused by low solar radiation (56%) and heavy rainfall (41%) considering data from all research stations, with a 3% residual not explained by these variables. At individual research stations, the impacts of low solar radiation on grain number per unit area varied from 4% to 33%, impacts of heavy rainfall varied from 1% to 15%, and the impact of ear

blight was less than 1%. For grain size, the main causes of decline were anoxia (51%), fungal foliar disease (21%), ear blight (19%), and low solar radiation during grain filling (6%), with 3% not explained by these variables. Apart from research station 8 where there was no waterlogging, the impact of anoxia on the decrease in grain size varied from 2% to 20%. Grain size was also affected by fungal foliar diseases, ear blight, and low solar radiation, which caused grain size decreases of up to 8% at individual research stations. The relatively low impact of low solar radiation on grain size (8% at most) compared to grain number (33% at most) was consistent with simulation results from the DSSAT-Nwheat model (Figures S16 and S17).

The contribution to grain yield of individual limiting factors in 2016 was estimated by combining the contributions to grain number per unit area and grain size. Overall, when ranked by the size of impact, the 2016 yield drop can primarily be explained by reduced solar radiation around anthesis (31%), anoxia during grain filling (26%), heavy rainfall events at anthesis (19%), fungal foliar diseases (11%), and ear blight during grain filling (10%), with 3% of the loss not explained (Figure 5).

3.6 | Increased frequency of adverse weather conditions for wheat yield under future climate

We used bias-adjusted climate projections from the CMIP6 subset to anticipate risks similar to the 2016 impacts over the shared socioeconomic pathway SSP5-8.5 for the 2020–2100 period. We thus assessed whether future climate change trends might change the frequencies of heavy rainfall and solar radiation around wheat anthesis, ear blight, fungal foliar diseases, and anoxia during grain filling, as experienced in 2016 (Figure 6, which shows the average climate projections for eight research station across the breadbasket of France). Results indicate that under the SSP5-8.5 scenario, heavy rainfall around anthesis is projected to become up to 100% more frequent after 2040 (Figure 6a), while small changes are possible in average solar radiation around anthesis, increasing by 5% by 2100 (Figure 6b). Similarly, under the SSP5-8.5 scenario, the frequency of ear blight would increase by 110% and fungal foliar diseases would increase by 50% by 2100 due to warmer winter and spring (Table S3). By contrast, anoxia during June to July, the grain-filling period, is projected to become up to 25% less frequent under the SSP5-8.5 scenario. All factors which caused the large yield drop in 2016 would become more pronounced with future climate change, but low solar radiation and anoxia would be limiting less often. Similar projections are expected in other regions of Europe and for different wheat anthesis dates (Figures S19 and S20). High decadal variability is shown for all projected weather-based index (Figure 6a–e), but particularly for heavy rainfall at anthesis (Figure 6a) and ear blight (Figure 6b), which may be linked to the uncertainties of the ensemble means based on the CMIP6 global climate models.

Extreme low wheat yields are here statistically defined as the <2nd percentile of occurrence of simulated wheat yields during 1960–2020, thus with a probability which occurred once in 60 years in the past (corresponding to the frequency of the 2016 wheat yield failure). With increasing solar radiation and heavy rainfall during anthesis, the frequency of extreme low wheat grain number due to climatic factors that occurred in 2016 is projected to remain unchanged (Figure 6f). However, with increasing plant disease, extremely low wheat grain size and hence grain yields are projected to become five times more frequent by the end of the century under the SSP5-8.5 scenario (Figure 6g,h). Similar results are expected under the SSP5-2.6 scenario (Figure S21). Yet, these projections may vary according to the modeling approach used (Figure S33).

4 | DISCUSSION

Grain yield in wheat is determined by grain number per unit area and average single grain size. There is a negative relationship between the two components, which suggests that wheat partially compensates during development for variation in grain number per unit area by modifying grain size once grain number is determined (Zhang et al., 2010). However, we showed here that the large and sudden drop in wheat yield in 2016 in France occurred due to simultaneous drops in grain number per unit area and in average single grain size due to a combination of adverse climate events (Figure S22). The low grain number was partly driven by low solar radiation around anthesis in France in spring of 2016. An 18% decrease in grain number due to 65% less solar radiation centered around anthesis was reported by Fischer (1985). A shading experiment by Yang et al. (2020) showed a 58% drop in grain number when two wheat cultivars were 90% shaded during the early microspore stage of flower development when grain number is determined. These reports are in accordance with the estimates from regression and crop simulation models presented here. Broadly compared to other years before and after, only one-fifth of the solar radiation was received during the crucial flowering period with one-third fewer grains formed in some of the experimental locations in 2016 (Figures S4 and S5). High rainfall is often linked to low grain numbers due to its indirect effect on plant disease spread and nitrogen leaching (Mäkinen et al., 2018). From the data presented here, it is more likely that the intense rainfall around anthesis in 2016 in France directly caused flower abortion (Lawson & Rands, 2019) or increased lodging during anthesis (Fischer & Stapper, 1987; Niu et al., 2016).

Waterlogging, simply indicated here by water balance, was a widespread phenomenon in 2016, leading to flooding in wheat fields across the Seine River basin (Ben-Ari et al., 2018). Anoxia probably only occurred during the wheat grain-filling period. Marti et al. (2015) reported a grain yield decline of 20% due to 10–15 days of waterlogging with a high impact on grain number due to the excess of water just before anthesis. The timing of the impact on grain size is therefore different from that reported here. Fungal foliar diseases also reduced average wheat grain size, with ear blight and low solar radiation exacerbating the decrease. Similar effects of low radiation during different growth periods were observed by Shimoda

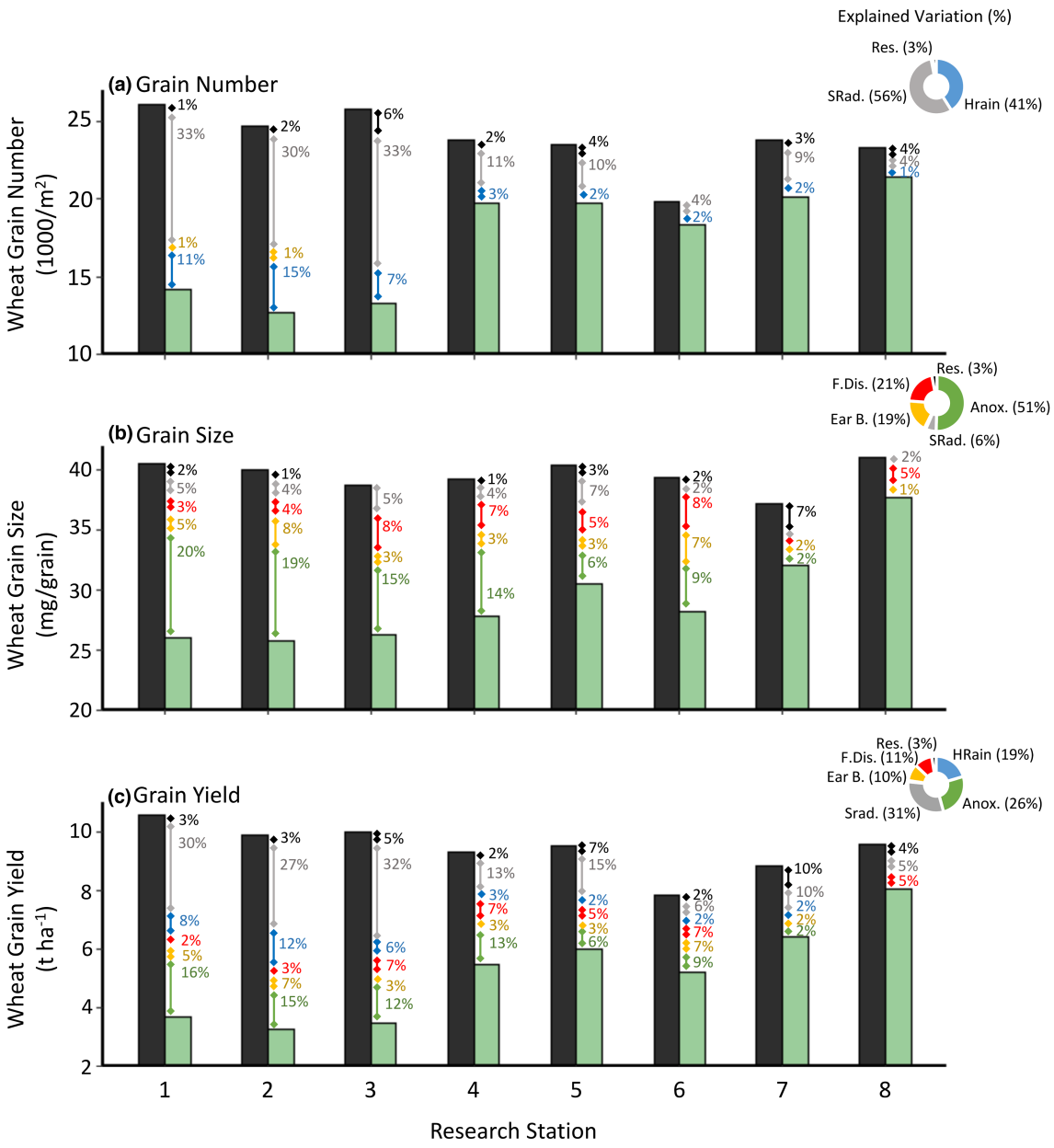

FIGURE 5 Causes of the extremely low wheat yield in France in 2016. Comparison of the observed (a) grain number per unit area, (b) average single grain size, and (c) grain yield reported in 2016 and the average of 2014, 2015, 2017, 2018, and 2019 harvests. The colored arrows represent the different causes of the 2016 decline in grain number, size, and yield, and the length represents the magnitude of each contribution. The donut charts in the right upper corner of each panel show ANOVA (mean of squares) results with the amount of variation in (a) grain number per unit area, (b) average single grain size, and (c) grain yield explained by different factors in 2016 across all research stations: SRad., solar radiation; Hrain, heavy rainfall; F. Dis., foliar diseases; Ear B., ear blight; Anox., anoxia; and Res., residual. The research stations are as follows: 1, Égreville; 2, Chevry; 3, Saint-Quentin; 4, Saint-Florent; 5, Fagnières; 6, Issoudun; 7, Barbarey-Saint-Sulpice; and 8, Rots.

and Sugikawa (2020) and estimated by Asseng et al. (2017) using the same wheat crop model as in this study. In the model, the determination of grain number is source limited while grain growth beyond the onset of grain filling is often sink limited (Asseng et al., 2017). In the absence of any disease control, up to 30% decline in yield may be caused by ear blight (Shah et al., 2018) and up to 50% by septoria blotch (Fones & Gurr, 2015). The impact of plant diseases estimated here using regression models was smaller. However, resistant cultivars or fungicide applications during the growing season (Fones & Gurr, 2015; Shah et al., 2018) (up to three applications are common practice in Western Europe including the experimental unit treatments in France analyzed here) may have limited the wheat yield decline due to these diseases to between 5% and 10%.

European countries are global hotspots for climate change-driven compound events with the potential to cause severe impacts on agriculture (Ranasinghe et al., 2021; Ridder et al., 2020). Recent studies showed that drought and heat stress during wheat anthesis and grain filling would become more frequent by 2100 with climate change, in

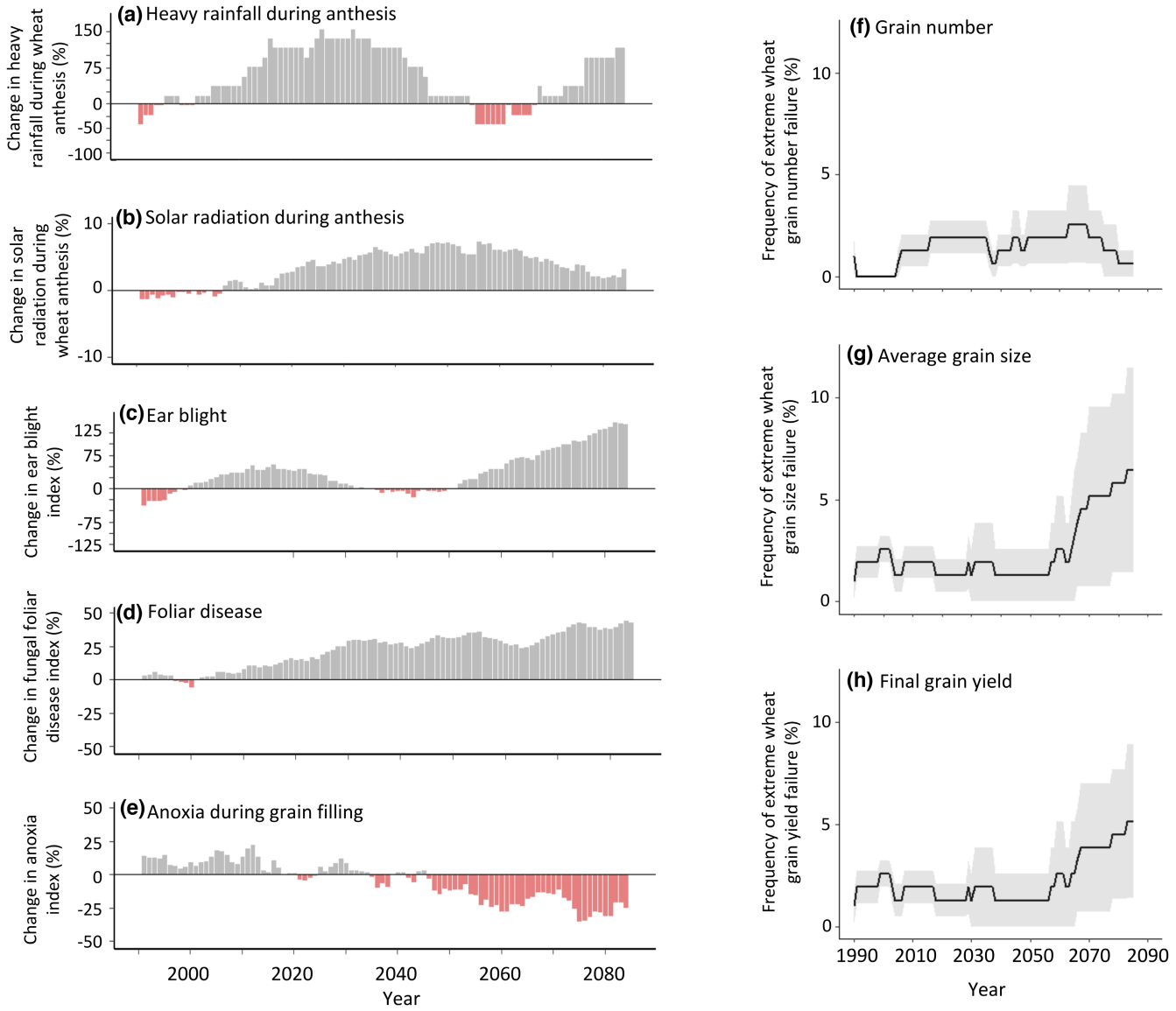

FIGURE 6 Projected future frequency of the extreme weather on the 2016 wheat yield failure in France. Estimated running mean change for future 30 years of (a) heavy rainfall (daily rainfall >20 mm) at ±5 days around anthesis, (b) solar radiation at ±15 days around anthesis, (c) ear blight index, (d) fungal foliar disease index, and (e) anoxia index during grain filling in relation to the reference period 1960–2020. Estimated running mean change for future 30 years frequency of extremely low wheat (f) grain number per unit area, (g) average single grain size, and (c) grain yield from 1990 to 2085, with each year as the middle of a 30-year period. (a–e) Bars are ensemble means based on five bias-adjusted CMIP6 global climate models (GCMs) for SSP5-8.5. (f–h) Lines are ensemble means based on five bias-adjusted CMIP6 GCMs for SSP5-8.5 (lines) and shading shows ±1 SE. In the simulations, anthesis was fixed as 1 June, and the anoxia index was calculated every year from 1 June to 31 July. CMIP6 GCMs for SSP5-8.5 data are an average of climate projections for the following eight research stations: 1, Égreville; 2, Chevry; 3, Saint-Quentin; 4, Saint-Florent; 5, Fagnières; 6, Issoudun; 7, Barbarey-Saint-Sulpice; and 8, Rots. Individual results for these research stations and other locations in Europe, as well as with different anthesis dates, are shown in Figures S19 and S20, respectively. Climate projections for monthly maximum and minimum temperature, solar radiation, and rainfall, are shown in Figure S18. Projected future frequency of the extreme weather on the 2016 wheat yield failure in France for SSP5-2.6 is shown in Figure S21. Thresholds for heavy rainfall (daily rainfall >20 mm) are similar in both observed climate and climate models (Figure S9), and modeled weather-based indices have similar distribution in both observed climate and climate models (Figure S10).

many European wheat-growing countries (Trnka et al., 2014, 2019; Webber et al., 2018). This is consistent with our projections of less anoxia from rainfall during wheat grain filling by 2100. However, wheat diseases and heavy rainfall around anthesis, which together caused the majority of the wheat yield decline in 2016 in France, are both projected to become more frequent with climate change in the region (Figure 6). Heavy rainfall has already become more intense in Central Europe (Zeder & Fischer, 2020). Therefore, if climate extremes of drought and heat stress during wheat anthesis and grain filling are compounded with elevated pressure from disease and more heavy early rainfall events, future episodes of extremely low wheat production in Western Europe are to be expected. This

parallels recent widespread wheat crop failures in other countries of Europe and the world. For example, in 2018, a combination of a warm, wet winter, with increased wheat disease pressure, followed by a severely hot and dry summer in central-northern Europe (Beillouin et al., 2020; Moravec et al., 2021; Webber et al., 2020) caused the national wheat yield of France to drop by 10%. This was also the lowest wheat-yielding year in the recent history of Germany (after trend correction, Figure S25) and of many northern European countries (Beillouin et al., 2020; Webber et al., 2020), with a total wheat shortfall of 13 million tons in the European Union compared to 2017. These examples of climate change driving extremely low wheat production seasons in other parts of the world demonstrate the risks of simultaneous global breadbasket failures (Gaupp et al., 2020), and have implications for global food security. For example, the simultaneous wheat production failures in several wheat-exporting countries in 2008 contributed to food riots across many countries in the world (IMF, 2008). And, the heatwave in Russia and Ukraine in 2010 decimates 24 million tons of wheat, contributing to a 50% spike in global wheat price this year (FAO stat, 2022).

The simultaneous occurrence of multiple limiting impacts often makes it difficult to forecast extremely low wheat-yielding seasons. Forecasting seasons like 2016 in France are often hampered by the poor representation of waterlogging and plant disease in both crop simulation and statistical models (Ben-Ari et al., 2018). New routines accounting for plant diseases (Berton Ferreira et al., 2021; Bregaglio et al., 2021) and waterlogging impact (Liu et al., 2021) need to be developed and integrated into crop simulation models to capture the extent of such compounding factors. In the meantime, the simple relationships developed here capture some of the physiological impacts of waterlogging and diseases, as first steps toward a more comprehensive cropping systems analysis.

Our modeling approach included some assumptions. Factors affecting grain number per unit area were rather simply separated from those affecting average single grain size, even though potential grain size is also determined during the period when grain number per unit area is set (Acreche & Slafer, 2006; Calderini et al., 2021). Even with the large and detailed dataset studied, the available measurements did not allow us to quantify the impact of climate factors on the potential grain size during anthesis. Also, the anthesis dates and grain-filling duration for the future climate change impact analysis were kept constant, but these timings might change with increasing temperatures or future cultivars. Depending on the direction of the changes in anthesis date and grain-filling period (whether earlier anthesis and shorter grain filling with current cultivars or unaltered or later anthesis with possible future cultivars [Asseng et al., 2019]), the overall impact might vary.

While the data analysis focused on the breadbasket of France, the approach used here could be extended to other countries in Western Europe which suffered similar weather anomalies during the wheat cropping season of 2016 (Figure 1). Our framework provides a basis for future improvement of the prediction capacity of crop simulation models and yields forecast systems, and for developing wheat cultivars with an increased ecophysiological capacity to grow in complex environments, like those in 2016 in France. Forecasting and planning for such compound yield-reducing events may to some extent mitigate the instability of future grain production under more extreme climates.

ACKNOWLEDGMENTS

The authors thank ARVALIS-Institut du Végétal for performing all the field experiments and for the financial support of this study. R.S.N.J. acknowledges support from the Prince of Albert II of Monaco foundation through the IPCC Scholarship Program. The contents of this manuscript are solely the liability of R.S.N.J. and under no circumstances may be considered a reflection of the position of the Prince Albert II of Monaco Foundation and/or the IPCC. P.M. acknowledges support from the Agriculture and Forestry in the Face of Climate Change: Adaptation and Mitigation (CLIMAE) Metaprogram of the French National Research Institute for Agriculture, Food and Environment (INRAE). Support for A.C.R. was provided by the NASA Earth Sciences Directorate support of the GISS Climate Impacts Group. F.E. acknowledges support from the Deutsche Forschungsgemeinschaft (DFG, German Research Foundation) under Germany's Excellence Strategy – EXC 2070 – 390732324 (PhenoRob). Open Access funding enabled and organized by Projekt DEAL.

CONFLICT OF INTEREST STATEMENT

The authors declare no conflict of interest.

DATA AVAILABILITY STATEMENT

The data that support the findings of this study are available at https://doi.org/10.5061/dryad.fxpnvx0x1.

ORCID

Rogério de S. Nóia Júnior https://orcid.org/0000-0002-4096-7588
Jean-Pierre Cohan https://orcid.org/0000-0003-2117-7027
Pierre Martre https://orcid.org/0000-0002-7419-6558
Marijn van der Velde https://orcid.org/0000-0002-9103-7081
Heidi Webber https://orcid.org/0000-0001-8301-5424
Frank Ewert https://orcid.org/0000-0002-4392-8154
Alex C. Ruane https://orcid.org/0000-0002-5582-9217
Gustavo A. Slafer https://orcid.org/0000-0002-1766-4247
Senthold Asseng https://orcid.org/0000-0002-7583-3811

REFERENCES

Acreche, M. M., & Slafer, G. A. (2006). Grain weight response to increases in number of grains in wheat in a Mediterranean area. *Field Crops Research*, *98*(1), 52–59. https://doi.org/10.1016/j.fcr.2005.12.005

Asseng, S., Foster, I., & Turner, N. C. (2011). The impact of temperature variability on wheat yields. *Global Change Biology*, *17*(2), 997–1012. https://doi.org/10.1111/j.1365-2486.2010.02262.x

Asseng, S., Kassie, B. T., Labra, M. H., Amador, C., & Calderini, D. F. (2017). Simulating the impact of source-sink manipulations in wheat. *Field Crops Research*, *202*, 47–56. https://doi.org/10.1016/j.fcr.2016.04.031

Asseng, S., Martre, P., Maiorano, A., Rötter, R. P., O'Leary, G. J., Fitzgerald, G. J., Girousse, C., Motzo, R., Giunta, F., Babar, M. A., Reynolds, M. P., Kheir, A. M. S., Thorburn, P. J., Waha, K., Ruane, A. C., Aggarwal, P. K., Ahmed, M., Balkovič, J., Basso, B., … Ewert, F. (2019). Climate change impact and adaptation for wheat protein. *Global Change Biology*, *25*(1), 155–173. https://doi.org/10.1111/gcb.14481

Bailey, R., Benton, T. G., Challinor, A., Elliott, J., & Gustafson, D. (2015). *Extreme weather and resilience of the global food system*. The Global Food Security Programme.

Battisti, D. S., & Naylor, R. L. (2009). Historical warnings of future food insecurity with unprecedented seasonal heat. *Science*, *323*(5911), 240–244. https://doi.org/10.1126/science.1164363

Beillouin, D., Schauberger, B., Bastos, A., Ciais, P., & Makowski, D. (2020). Impact of extreme weather conditions on European crop production in 2018. *Philosophical Transactions of the Royal Society, B: Biological Sciences*, *375*(1810), 20190510. https://doi.org/10.1098/rstb.2019.0510

Ben-Ari, T., Boé, J., Ciais, P., Lecerf, R., van der Velde, M., & Makowski, D. (2018). Causes and implications of the unforeseen 2016 extreme yield loss in the breadbasket of France. *Nature Communications*, *9*(1), 1627. https://doi.org/10.1038/s41467-018-04087-x

Berton Ferreira, T., Pavan, W., Cunha Fernandes, J. M., Asseng, S., Antunes de Oliveira, F. A., Amaral Ho¨lbig, C., Noleto Luz Pequeno, D., Dalmago, G. A., Lazaretti Zanatta, A., & Hoogenboom, G. (2021). Coupling a Pest and disease damage module with CSM-NWheat—A wheat crop simulation model. *Transactions of the ASABE*, *64*, 2061–2071. https://doi.org/10.13031/trans.14586

Bevacqua, E., De Michele, C., Manning, C., Couasnon, A., Ribeiro, A. F. S., Ramos, A. M., Vignotto, E., Bastos, A., Blesić, S., Durante, F., Hillier, J., Oliveira, S. C., Pinto, J. G., Ragno, E., Rivoire, P., Saunders, K., van der Wiel, K., Wu, W., Zhang, T., & Zscheischler, J. (2021). Guidelines for studying diverse types of compound weather and climate events. *Earth's Future*, *9*(11), e2021EF002340. https://doi.org/10.1029/2021EF002340

Bregaglio, S., Willocquet, L., Kersebaum, K. C., Ferrise, R., Stella, T., Ferreira, T. B., Pavan, W., Asseng, S., & Savary, S. (2021). Comparing process-based wheat growth models in their simulation of yield losses caused by plant diseases. *Field Crops Research*, *265*, 108108. https://doi.org/10.1016/j.fcr.2021.108108

Bussay, A., van der Velde, M., Fumagalli, D., & Seguini, L. (2015). Improving operational maize yield forecasting in Hungary. *Agricultural Systems*, *141*, 94–106. https://doi.org/10.1016/j.agsy.2015.10.001

Calderini, D. F., Castillo, F. M., Arenas-M, A., Molero, G., Reynolds, M. P., Craze, M., Bowden, S., Milner, M. J., Wallington, E. J., Dowle, A., Gomez, L. D., & McQueen-Mason, S. J. (2021). Overcoming the trade-off between grain weight and number in wheat by the ectopic expression of expansin in developing seeds leads to increased yield potential. *New Phytologist*, *230*(2), 629–640. https://doi.org/10.1111/nph.17048

Ceglar, A., van der Wijngaart, R., de Wit, A., Lecerf, R., Boogaard, H., Seguini, L., van den Berg, M., Toreti, A., Zampieri, M., Fumagalli, D., & Baruth, B. (2019). Improving WOFOST model to simulate winter wheat phenology in Europe: Evaluation and effects on yield. *Agricultural Systems*, *168*, 168–180. https://doi.org/10.1016/j.agsy.2018.05.002

Cohan, J.-P., Le Souder, C., Guicherd, C., Lorgeou, J., Du Cheyron, P., Bonnefoy, M., Decarrier, A., Piraux, F., & Laurent, F. (2019). Combining breeding traits and agronomic indicators to characterize the impact of cultivar on the nitrogen use efficiency of bread wheat. *Field Crops Research*, *242*, 107588. https://doi.org/10.1016/j.fcr.2019.107588

Eyring, V., Bony, S., Meehl, G. A., Senior, C. A., Stevens, B., Stouffer, R. J., & Taylor, K. E. (2016). Overview of the coupled model Intercomparison project phase 6 (CMIP6) experimental design and organization. *Geoscientific Model Development*, *9*(5), 1937–1958. https://doi.org/10.5194/gmd-9-1937-2016

FAO stat. (2022). *FAOSTAT: FAO statistical databases*. FAO Stat. http://www.fao.org/faostat/en/#home

Fischer, R. A. (1985). Number of kernels in wheat crops and the influence of solar radiation and temperature. *The Journal of Agricultural Science*, *105*(2), 447–461. https://doi.org/10.1017/S0021859600056495

Fischer, R. A., & Stapper, M. (1987). Lodging effects on high-yielding crops of irrigated semidwarf wheat. *Field Crops Research*, *17*(3), 245–258. https://doi.org/10.1016/0378-4290(87)90038-4

Fones, H., & Gurr, S. (2015). The impact of Septoria tritici blotch disease on wheat: An EU perspective. *Fungal Genetics and Biology*, *79*, 3–7. https://doi.org/10.1016/j.fgb.2015.04.004

Gaupp, F., Hall, J., Hochrainer-Stigler, S., & Dadson, S. (2020). Changing risks of simultaneous global breadbasket failure. *Nature Climate Change*, *10*(1), 54–57. https://doi.org/10.1038/s41558-019-0600-z

Hoag, H. (2014). Russian summer tops "universal" heatwave index. *Nature*, *16*, 250–252. https://doi.org/10.1038/nature.2014.16250

Igrejas, G., & Branlard, G. (2020). The importance of wheat. In G. Igrejas & G. Branlard (Eds.), *Wheat quality for improving processing and human health* (pp. 1–7). Springer International Publishing. https://doi.org/10.1007/978-3-030-34163-3_1

IMF. (2008). *International Monetary Fund: Food and fuel prices: Recent developments, macroeconomic impact, and policy responses*.

IPCC. (2021). Technical summary. Contribution of working group I to the sixth assessment report of the intergovernmental panel on climate change. In V. Masson-Delmotte, P. Zhai, A. Pirani, S. L. Connors, C. Péan, S. Berger, N. Caud, Y. Chen, L. Goldfarb, M. I. Gomis, M. Huang, K. Leitzell, E. Lonnoy, J. B. R. Matthews, T. K. Maycock, T. Waterfield, O. Yelekçi, R. Yu, & B. Zhou (Eds.), *Climate Change 2021: The Physical Science Basis*.

Jägermeyr, J., Müller, C., Ruane, A. C., Elliott, J., Balkovic, J., Castillo, O., Faye, B., Foster, I., Folberth, C., Franke, J. A., Fuchs, K., Guarin, J. R., Heinke, J., Hoogenboom, G., Iizumi, T., Jain, A. K., Kelly, D., Khabarov, N., Lange, S., … Rosenzweig, C. (2021). Climate impacts on global agriculture emerge earlier in new generation of climate and crop models. *Nature Food*, *2*, 873–885. https://doi.org/10.1038/s43016-021-00400-y

Justes, E., Mary, B., Meynard, J.-M., Machet, J.-M., & Thelier-Huche, L. (1994). Determination of a critical nitrogen dilution curve for Winter wheat crops. *Annals of Botany*, *74*(4), 397–407. https://doi.org/10.1006/anbo.1994.1133

Kassie, B. T., Asseng, S., Porter, C. H., & Royce, F. S. (2016). Performance of DSSAT-Nwheat across a wide range of current and future growing conditions. *European Journal of Agronomy*, *81*, 27–36. https://doi.org/10.1016/j.eja.2016.08.012

Lange, S. (2019). Trend-preserving bias adjustment and statistical downscaling with ISIMIP3BASD (v1.0). *Geoscientific Model Development*, *12*(7), 3055–3070. https://doi.org/10.5194/gmd-12-3055-2019

Lawson, D. A., & Rands, S. A. (2019). The effects of rainfall on plant–pollinator interactions. *Arthropod-Plant Interactions*, *13*(4), 561–569. https://doi.org/10.1007/s11829-019-09686-z

Lecerf, R., Ceglar, A., López-Lozano, R., van der Velde, M., & Baruth, B. (2019). Assessing the information in crop model and meteorological indicators to forecast crop yield over Europe. *Agricultural Systems*, *168*, 191–202. https://doi.org/10.1016/j.agsy.2018.03.002

Lischeid, G., Webber, H., Sommer, M., Nendel, C., & Ewert, F. (2022). Machine learning in crop yield modelling: A powerful tool, but no surrogate for science. *Agricultural and Forest Meteorology*, *312*, 108698. https://doi.org/10.1016/j.agrformet.2021.108698

Liu, B., Martre, P., Ewert, F., Porter, J. R., Challinor, A. J., Müller, C., Ruane, A. C., Waha, K., Thorburn, P. J., Aggarwal, P. K., Ahmed, M., Balkovič, J., Basso, B., Biernath, C., Bindi, M., Cammarano, D., De Sanctis, G., Dumont, B., Espadafor, M., … Asseng, S. (2019). Global wheat production with 1.5 and 2.0°C above pre-industrial warming. *Global Change Biology*, *25*(4), 1428–1444. https://doi.org/10.1111/gcb.14542

Liu, K., Harrison, M. T., Archontoulis, S. V., Huth, N., Yang, R., Liu, D. L., Yan, H., Meinke, H., Huber, I., Feng, P., Ibrahim, A., Zhang, Y., Tian, X., & Zhou, M. (2021). Climate change shifts forward flowering and reduces crop waterlogging stress. *Environmental Research Letters*, *16*(9), 94017. https://doi.org/10.1088/1748-9326/ac1b5a

Madgwick, J. W., West, J. S., White, R. P., Semenov, M. A., Townsend, J. A., Turner, J. A., & Fitt, B. D. L. (2011). Impacts of climate change on wheat anthesis and fusarium ear blight in the UK. *European Journal of Plant Pathology*, *130*(1), 117–131. https://doi.org/10.1007/s10658-010-9739-1

Mäkinen, H., Kaseva, J., Trnka, M., Balek, J., Kersebaum, K. C., Nendel, C., Gobin, A., Olesen, J. E., Bindi, M., Ferrise, R., Moriondo, M., Rodríguez, A., Ruiz-Ramos, M., Takáč, J., Bezák, P., Ventrella, D., Ruget, F., Capellades, G., & Kahiluoto, H. (2018). Sensitivity of European wheat to extreme weather. *Field Crops Research*, *222*, 209–217. https://doi.org/10.1016/j.fcr.2017.11.008

Marti, J., Savin, R., & Slafer, G. A. (2015). Wheat yield as affected by length of exposure to waterlogging during stem elongation. *Journal of Agronomy and Crop Science*, *201*(6), 473–486. https://doi.org/10.1111/jac.12118

Martre, P., Wallach, D., Asseng, S., Ewert, F., Jones, J. W., Rötter, R. P., Boote, K. J., Ruane, A. C., Thorburn, P. J., Cammarano, D., Hatfield, J. L., Rosenzweig, C., Aggarwal, P. K., Angulo, C., Basso, B., Bertuzzi, P., Biernath, C., Brisson, N., Challinor, A. J., … Wolf, J. (2015). Multimodel ensembles of wheat growth: Many models are better than one. *Global Change Biology*, *21*(2), 911–925. https://doi.org/10.1111/gcb.12768

Menze, B. H., Kelm, B. M., Masuch, R., Himmelreich, U., Bachert, P., Petrich, W., & Hamprecht, F. A. (2009). A comparison of random forest and its Gini importance with standard chemometric methods for the feature selection and classification of spectral data. *BMC Bioinformatics*, *10*(1), 213. https://doi.org/10.1186/1471-2105-10-213

Moravec, V., Markonis, Y., Rakovec, O., Svoboda, M., Trnka, M., Kumar, R., & Hanel, M. (2021). Europe under multi-year droughts: How severe was the 2014–2018 drought period? *Environmental Research Letters*, *16*(3), 34062. https://doi.org/10.1088/1748-9326/abe828

Niu, L., Feng, S., Ding, W., & Li, G. (2016). Influence of speed and rainfall on large-scale wheat lodging from 2007 to 2014 in China. *PLoS One*, *11*(7), e0157677. https://doi.org/10.1371/journal.pone.0157677

Nóia Júnior, R. d. S., Martre, P., Finger, R., van der Velde, M., Ben-Ari, T., Ewert, F., Webber, H., Ruane, A. C., & Asseng, S. (2021). Extreme lows of wheat production in Brazil. *Environmental Research Letters*, *16*(10), 104025. https://doi.org/10.1088/1748-9326/ac26f3

O'Neill, B. C., Carter, T. R., Ebi, K., Harrison, P. A., Kemp-Benedict, E., Kok, K., Kriegler, E., Preston, B. L., Riahi, K., Sillmann, J., van Ruijven, B. J., van Vuuren, D., Carlisle, D., Conde, C., Fuglestvedt, J., Green, C., Hasegawa, T., Leininger, J., Monteith, S., & Pichs-Madruga, R. (2020). Achievements and needs for the climate change scenario framework. *Nature Climate Change*, *10*(12), 1074–1084. https://doi.org/10.1038/s41558-020-00952-0

Pang, G., Xu, Z., Wang, T., Cong, X., & Wang, H. (2018). Photosynthetic light response characteristics of winter wheat at heading and flowering stages under saline water irrigation. *IOP Conference Series: Earth and Environmental Science*, *170*, 52031. https://doi.org/10.1088/1755-1315/170/5/052031

Perez, I. (2013). *Climate change and rising food prices heightened Arab spring*. Scientific American: Sustainability.

R Core Team. (2017). *R: A language and environment for statistical computing*. R Foundation for Statistical Computing (p. {ISBN} 3–900051–07-0). http://www.R-project.org/

Ranasinghe, R., Ruane, A. C., Vautard, R., Arnell, N., Coppola, E., Cruz, F. A., Dessai, S., Islam, A. S., Rahimi, M., Carrascal, D. R., Sillmann, J., Sylla, M. B., Tebaldi, C., Wang, W., & Zaaboul, R. (2021). Chapter 12: Climate change information for regional impact and for risk assessment. In V. Masson-Delmotte, P. Zhai, A. Pirani, S. L. Connors, C. Péan, S. Berger, N. Caud, Y. Chen, L. Goldfarb, M. I. Gomis, M. Huang, K. Leitzell, E. Lonnoy, J. B. R. Matthews, T. K. Maycock, T. Waterfield, O. Yelekçi, R. Yu, & B. Zhou (Eds.), *Climate change 2021: The physical science basis. Contribution of Working Group I to the Sixth Assessment Report of the Intergovernmental Panel on Climate Change*, *August 2021* (pp. 351–364).

Raymond, C., Horton, R. M., Zscheischler, J., Martius, O., AghaKouchak, A., Balch, J., Bowen, S. G., Camargo, S. J., Hess, J., Kornhuber, K., Oppenheimer, M., Ruane, A. C., Wahl, T., & White, K. (2020). Understanding and managing connected extreme events. *Nature Climate Change*, *10*(7), 611–621. https://doi.org/10.1038/s41558-020-0790-4

Ridder, N. N., Pitman, A. J., Westra, S., Ukkola, A., Do, H. X., Bador, M., Hirsch, A. L., Evans, J. P., Di Luca, A., & Zscheischler, J. (2020). Global hotspots for the occurrence of compound events. *Nature Communications*, *11*(1), 5956. https://doi.org/10.1038/s41467-020-19639-3

Rosenzweig, C., Jones, J. W., Hatfield, J. L., Ruane, A. C., Boote, K. J., Thorburn, P., Antle, J. M., Nelson, G. C., Porter, C., Janssen, S., Asseng, S., Basso, B., Ewert, F., Wallach, D., Baigorria, G., & Winter, J. M. (2013). The agricultural model Intercomparison and improvement project (AgMIP): Protocols and pilot studies. *Agricultural and Forest Meteorology*, *170*, 166–182. https://doi.org/10.1016/j.agrformet.2012.09.011

Rötter, R. P., Hoffmann, M. P., Koch, M., & Müller, C. (2018). Progress in modelling agricultural impacts of and adaptations to climate change. *Current Opinion in Plant Biology*, *45*, 255–261. https://doi.org/10.1016/j.pbi.2018.05.009

Ruane, A. C., Phillips, M., Müller, C., Elliott, J., Jägermeyr, J., Arneth, A., Balkovic, J., Deryng, D., Folberth, C., Iizumi, T., Izaurralde, R. C., Khabarov, N., Lawrence, P., Liu, W., Olin, S., Pugh, T. A. M., Rosenzweig, C., Sakurai, G., Schmid, E., … Yang, H. (2021). Strong regional influence of climatic forcing datasets on global crop model ensembles. *Agricultural and Forest Meteorology*, *300*, 108313. https://doi.org/10.1016/j.agrformet.2020.108313

Shah, L., Ali, A., Yahya, M., Zhu, Y., Wang, S., Si, H., Rahman, H., & Ma, C. (2018). Integrated control of fusarium head blight and deoxynivalenol mycotoxin in wheat. *Plant Pathology*, *67*(3), 532–548. https://doi.org/10.1111/ppa.12785

Shew, A. M., Tack, J. B., Nalley, L. L., & Chaminuka, P. (2020). Yield reduction under climate warming varies among wheat cultivars in South Africa. *Nature Communications*, *11*(1), 4408. https://doi.org/10.1038/s41467-020-18317-8

Shimoda, S., & Sugikawa, Y. (2020). Grain-filling response of winter wheat (Triticum aestivum L.) to post-anthesis shading in a humid climate. *Journal of Agronomy and Crop Science*, *206*(1), 90–100. https://doi.org/10.1111/jac.12370

Slafer, G. A., Elia, M., Savin, R., García, G. A., Terrile, I. I., Ferrante, A., Miralles, D. J., & González, F. G. (2015). Fruiting efficiency: An alternative trait to further rise wheat yield. *Food and Energy Security*, *4*(2), 92–109. https://doi.org/10.1002/fes3.59

te Beest, D. E., Shaw, M. W., Pietravalle, S., & van den Bosch, F. (2009). A predictive model for early-warning of Septoria leaf blotch on winter wheat. *European Journal of Plant Pathology*, *124*(3), 413–425. https://doi.org/10.1007/s10658-009-9428-0

Trnka, M., Feng, S., Semenov, M. A., Olesen, J. E., Kersebaum, K. C., Rötter, R. P., Semerádová, D., Klem, K., Huang, W., Ruiz-Ramos, M., Hlavinka, P., Meitner, J., Balek, J., Havlík, P., & Büntgen, U. (2019). Mitigation efforts will not fully alleviate the increase in water scarcity occurrence probability in wheat-producing areas. *Science Advances*, *5*(9), eaau2406. https://doi.org/10.1126/sciadv.aau2406

Trnka, M., Rötter, R. P., Ruiz-Ramos, M., Kersebaum, K. C., Olesen, J. E., Žalud, Z., & Semenov, M. A. (2014). Adverse weather conditions for European wheat production will become more frequent with climate change. *Nature Climate Change*, *4*(7), 637–643. https://doi.org/10.1038/nclimate2242

van der Velde, M., & Nisini, L. (2019). Performance of the MARS-crop yield forecasting system for the European Union: Assessing accuracy, in-season, and year-to-year improvements from 1993 to 2015. *Agricultural Systems*, *168*, 203–212. https://doi.org/10.1016/j.agsy.2018.06.009

van der Velde, M., Lecerf, R., d'Andrimont, R., & Ben-Ari, T. (2020). *Chapter 8—Assessing the France 2016 extreme wheat production loss—Evaluating our operational capacity to predict complex compound events*. In J. Sillmann, S. Sippel, & S. Russo (Eds.), (pp. 139–158). Elsevier. https://doi.org/10.1016/B978-0-12-814895-2.00009-4

Wang, E., Martre, P., Zhao, Z., Ewert, F., Maiorano, A., Rötter, R. P., Kimball, B. A., Ottman, M. J., Wall, G. W., White, J. W., Reynolds, M. P., Alderman, P. D., Aggarwal, P. K., Anothai, J., Basso, B., Biernath, C., Cammarano, D., Challinor, A. J., De Sanctis, G., … Asseng, S. (2017). The uncertainty of crop yield projections is reduced by improved temperature response functions. *Nature Plants*, *3*(8), 17102. https://doi.org/10.1038/nplants.2017.102

Webber, H., Ewert, F., Olesen, J. E., Müller, C., Fronzek, S., Ruane, A. C., Bourgault, M., Martre, P., Ababaei, B., Bindi, M., Ferrise, R., Finger, R., Fodor, N., Gabaldón-Leal, C., Gaiser, T., Jabloun, M., Kersebaum, K.-C., Lizaso, J. I., Lorite, I. J., … Wallach, D. (2018). Diverging importance of drought stress for maize and winter wheat in Europe. *Nature Communications*, *9*(1), 4249. https://doi.org/10.1038/s41467-018-06525-2

Webber, H., Lischeid, G., Sommer, M., Finger, R., Nendel, C., Gaiser, T., & Ewert, F. (2020). No perfect storm for crop yield failure in Germany. *Environmental Research Letters*, *15*(10), 104012. https://doi.org/10.1088/1748-9326/aba2a4

Webber, H., Martre, P., Asseng, S., Kimball, B., White, J., Ottman, M., Wall, G. W., De Sanctis, G., Doltra, J., Grant, R., Kassie, B., Maiorano, A., Olesen, J. E., Ripoche, D., Rezaei, E. E., Semenov, M. A., Stratonovitch, P., & Ewert, F. (2017). Canopy temperature for simulation of heat stress in irrigated wheat in a semi-arid environment: A multi-model comparison. *Field Crops Research*, *202*, 21–35. https://doi.org/10.1016/j.fcr.2015.10.009

Yang, H., Dong, B., Wang, Y., Qiao, Y., Shi, C., Jin, L., & Liu, M. (2020). Photosynthetic base of reduced grain yield by shading stress during the early reproductive stage of two wheat cultivars. *Scientific Reports*, *10*(1), 14353. https://doi.org/10.1038/s41598-020-71268-4

Zeder, J., & Fischer, E. M. (2020). Observed extreme precipitation trends and scaling in Central Europe. *Weather and Climate Extremes*, *29*, 100266. https://doi.org/10.1016/j.wace.2020.100266

Zhang, H., Turner, N. C., & Poole, M. L. (2010). Source - sink balance and manipulating sink - source relations of wheat indicate that the yield potential of wheat is sink-limited in high-rainfall zones. *Crop and Pasture Science*, *61*(10), 852. https://doi.org/10.1071/CP10161

Zscheischler, J., Martius, O., Westra, S., Bevacqua, E., Raymond, C., Horton, R. M., van den Hurk, B., AghaKouchak, A., Jézéquel, A., Mahecha, M. D., Maraun, D., Ramos, A. M., Ridder, N. N., Thiery, W., & Vignotto, E. (2020). A typology of compound weather and climate events. *Nature Reviews Earth & Environment*, *1*(7), 333–347. https://doi.org/10.1038/s43017-020-0060-z

SUPPORTING INFORMATION

Additional supporting information can be found online in the Supporting Information section at the end of this article.

How to cite this article: Nóia Júnior, R. d. S., Deswarte, J.-C., Cohan, J.-P., Martre, P., van der Velde, M., Lecerf, R., Webber, H., Ewert, F., Ruane, A. C., Slafer, G. A., & Asseng, S. (2023). The extreme 2016 wheat yield failure in France. *Global Change Biology*, *00*, 1–17. https://doi.org/10.1111/gcb.16662